Notes

Spin Crossover Bistability in Three Mutually Perpendicular Interpenetrated (4,4) Nets

Nicolás Moliner,[1a] Carmen Muñoz,[1b] Sylvie Létard,[1a] Xavier Solans,[1c] Nieves Menéndez,[1d] Antoine Goujon,[1d] François Varret,[1d] and José Antonio Real*,[1a]

Departament de Química Inorgánica, Facultat de Química de la Universitat de València, Dr. Moliner 50, E-46100 Burjassot, València, Spain, Departament de Física Aplicada, Universitat Politécnica de València Camino de Vera s/n E-46071 València, Spain, Departament de Cristallografía, Mineralogia i Dipòsits Minerals, Facultat de Geología, Universitat de Barcelona, E-08028 Barcelona, Spain, and Laboratoire d'Optique et Magnétisme, CNRS-Université de Versailles (UMR 8634), 45 Avenue des Etats Unis, 78035 Versailles, France

Received May 23, 2000

Introduction

Research into inorganic coordination polymers and their use in constructing novel solid-state architectures has become an area of increasing interest.[2,3] A question particularly relevant to this area is the degree and nature of interpenetration or polycatenation.[4] In addition, self-assembly of molecules driven by coordination to transition metal ions has become an important tool to explore the cooperative nature of the spin crossover phenomenon.[5] Particularly, bifunctional rodlike ligands of the polypyridine type have been proved to be particularly suitable both for metallosupramolecular chemistry as well as for the field of the spin crossover phenomenon. However, the number of polymeric spin crossover compounds reported up to now is still small.[6−10] Here we report the self-assembly of 1,4-bis(4-pyridyl)-butadiyne (bpb), a rigid bifunctional spacer ligand, and iron(II) ions. The resulting assembly of formula $[Fe(bpb)_2(NCS)_2]\cdot 0.5CH_3OH$ (**1**) is a singular example of the interpenetration of three mutually perpendicular nets undergoing the spin crossover phenomenon. This remarkable structural singularity has been envisaged,[4] but to our knowledge no reports in this respect are known to date.

Experimental Section

The synthesis of the ligand bpb was performed according to the method reported by Ciana and Haim.[11]

Preparation of 1. All the experiments were carried out under an argon atmosphere. $FeSO_4\cdot 7H_2O$ (0.25 mmol) was added to a solution of KNCS (0.5 mmol) in methanol (5 mL). The mixture was stirred at room temperature for 20 min, decanted off, and filtered. The resulting colorless 1:2 Fe^{II}/NCS^- solution was added dropwise to a methanol solution of bpb (0.5 mmol, 35 mL). After a week, slow evaporation of the resulting orange solution led to the formation of well-shaped dark red crystals of **1**. The crystals were separated and used for X-ray diffraction and physical measurements. Yield: ca. 74%. Anal. Calcd for $C_{30.5}H_{18}N_6O_{0.5}S_2Fe$: C, 61.42; H, 3.02; N, 14.09; S, 10.74. Found: C, 62.20; H, 2.89; N, 13.88; S, 10.25.

Magnetic Measurements. The variable temperature magnetic susceptibility measurements were carried out on microcrystalline samples using a Quantum Design MPMS2 SQUID susceptometer equipped with a 55 kG magnet and operating in the ranges of 0.1−1 T and 1.8−300 K. The susceptometer was calibrated with $(NH_4)_2Mn(SO_4)_2\cdot 12H_2O$. Experimental susceptibilities were corrected for diamagnetism of the constituent atoms by the use of Pascal's constants.

Mössbauer Spectra. The variable-temperature Mössbauer measurements were obtained on a constant-acceleration conventional spectrometer with a 25 mCi source of ^{57}Co (Rh matrix). Isomer shift values (IS) are given with respect to the metallic iron at room temperature. The absorber was a sample of about 100 mg of microcrystalline powder of **1** enclosed in a 2-cm-diameter cylindrical plastic sample holder, the size of which had been determined to optimize the absorption. Variable-temperature spectra were obtained in the 300−77 K range by using a MD306 Oxford cryostat, the thermal scanning being monitored by an Oxford ITC4 servocontrol device (±0.1 K accuracy).

X-ray Crystallography. A red cube-shaped crystal of **1** (0.1 × 0.1 × 0.1 mm) was mounted in air. The intensity data were collected at 293 K on a Marresearch MAR345 (MARSXDS data collection software) using graphite-monochromated Mo Kα radiation (λ = 0.710 69 Å) and the φ−scan technique. The $\Delta\varphi$ scan angle per frame was 3°. A total of 25 977 reflections were collected; 7438 were unique (R_{int} was 0.058), and there were 5142 observed reflections ($I > 2\sigma(I)$). The number of refined parameters was 394; $R_1 = 0.063$ and $wR_2 = 0.1904$. The structure was solved by direct methods using SHELXS-97[12] and refined by the full matrix least-squares method on F^2 using SHELXL-97.[13] Refinements assuming the formula as $C_{30}H_{16}FeN_6S_2$ gave four holes of volume equal to 159 Å^3. An analysis of the Fourier map of these holes showed two weak and broad peaks with an absolute integrated intensity equal to 7.4 e, so a disordered methanol molecule was assumed. The remaining hole (18 Å^3), the high equivalent thermal coefficient for the two atomic positions of methanol, and the shape of the peaks of the Fourier map indicate that the localization of this methanol molecule is not well-defined. The S(1), C(8), and C(10) atoms and the CH_3OH solvent molecule were found to have a half occupancy in their respective sites.

(1) (a) Departament de Química Inorgánica, Facultat de Química de la Universitat de València. (b) Departament de Física Aplicada, Universitat Politécnica de València. (c) Departament de Cristallografía, Mineralogia i Dipòsits Minerals, Facultat de Geología, Universitat de Barcelona. (d) Laboratoire d'Optique et Magnétisme, CNRS-Université de Versailles.
(2) Robson, R. In *Comprehensive Supramolecular Chemistry*; Atwood, J. L., Davies, J. E. D., MacNicol, D. D., Vögtle, F., Toda, F., Bishop, R., Eds.; Pergamon: Oxford, 1996; Vol. 6, p 733.
(3) Bowes, C. L.; Ozin, G. A. *Adv. Mater.* **1996**, *8*, 13.
(4) Batten, S. R.; Robson, R. *Angew. Chem., Int. Ed.* **1998**, *37*, 1460.
(5) Gütlich, P.; Hauser, A.; Spiering, H. *Angew. Chem., Int. Ed. Engl.* **1994,** *33*, 2024.
(6) Vreugdenhil, W.; van Diemen, J. H.; De Graaff, R. A. G.; Haasnoot, J. G.; Reedijk, J.; Kahn, O.; Zarembowitch, J. *Polyhedron* **1990**, *9*, 2971.
(7) Ozarowski, A.; Shunzhong, Y.; McGarvey, B. R.; Mislankar, A.; Drake, J. E. *Inorg. Chem.* **1991**, *30*, 3167.
(8) Real, J. A.; Andrés, E.; Muñoz, M. C.; Julve, M.; Granier, T.; Bousseksou, A.; Varret, F. *Science* **1995**, *268*, 265.
(9) Kahn, O.; Martinez, J. C. *Science* **1998**, *279*, 44.
(10) Garcia, Y.; Kahn, O.; Rabardel, L.; Chansou, B.; Salmon, L.; Tuchagues, J. P. *Inorg. Chem.* **1999**, *38*, 4663.
(11) Ciana, L. D.; Haim, A. *J. Heterocycl. Chem.* **1984**, *21*, 607.
(12) Sheldrick, G. M. SHELXS-97. *Acta Crystallogr.* **1990**, *A46*, 467.
(13) Sheldrick, G. M. *SHELXL-97*: *Program for the refinement of Crystal Structures*; University of Göttingen: Göttingen, Germany, 1997.

10.1021/ic0005588 CCC: $19.00
Published on Web 10/21/2000

Table 1. Crystallographic Data for **1**

empirical formula	$C_{30.5}H_{18}Fe_1N_6S_2O_{0.5}$
fw	596.48
space group	$P4_12_12$ (92)
a, Å	16.6280(10)
c, Å	22.7800(10)
V, Å^3	6298.5(6)
Z	8
T, K	293(2)
λ, Å	0.71069
μ, mm^{-1}	0.641
ρ_{calc}, g/cm^3	1.258
R1[a]	0.0634
wR2[b]	0.1904

[a] $R1 = \sum||F_o| - |F_c||/\sum|F_o|$. [b] $wR2 = [\sum[w(F_o^2 - F_c^2)^2/\sum[w(F_o^2)^2]]^{1/2}$; $w = 1/[\sigma^2(F_o^2) + (0.1063P)^2 + 1.3132P]$, where $P = (F_o^2 + 2F_c^2)/3$.

Table 2. Selected Bond Lengths [Å] and Angles [deg] for **1**

Bond Lengths			
Fe(1)−N(1)	2.047(4)	Fe(2)−N(21)	2.052(7)
Fe(1)−N(2)[b]	2.271(3)	Fe(2)−N(22)	2.270(5)
Fe(1)−N(3)	2.250(4)	Fe(2)−N(23)[d]	2.284(6)
S(1)−C(1)	1.727(10)	Fe(2)−N(24)	2.294(10)
N(1)−C(1)	1.196(9)	S(2)−C(21)	1.682(12)
		N(21)−C(21)	1.183(12)
		S(3)−C(36)	1.680(10)
		N(24)−C(36)	1.265(10)

Bond Angles			
N(1)−Fe(1)−N(1)[a]	179.3(2)	N(21)−Fe(2)−N(22)	87.91(13)
N(1)−Fe(1)−N(2)	92.82(15)	N(21)−Fe(2)−N(23)[d]	90.06(16)
N(1)−Fe(1)−N(3)[b]	92.98(19)	N(21)−Fe(2)−N(24)	180.0(2)
N(1)−Fe(1)−N(2)[a]	86.64(14)	N(22)−Fe(2)−N(22)[a]	175.8(3)
N(1)−Fe(1)−N(3)[c]	87.54(19)	N(22)−Fe(2)−N(23)[d]	91.52(19)
N(2)−Fe(1)−N(2)[a]	87.71(16)	N(22)[a]−Fe(2)−N(23)[d]	88.5(2)
N(2)−Fe(1)−N(3)[b]	173.96(16)	N(22)−Fe(2)−N(24)	92.11(13)
N(2)−Fe(1)−N(3)[c]	90.93(15)	N(23)[d]− Fe(2)−N(23)[e]	179.9(3)
N(3)[b]−Fe(1)−N(3)[c]	91.0(2)	N(23)[d]−Fe(2)−N(24)	89.95(15)

[a] Atom generated with symmetry operation $y, x, -z$. [b] Atom generated with symmetry operation $x - 1, y, z$. [c] Atom generated with symmetry operation $y, x - 1, -z$. [d] Atom generated with symmetry operation $-x + 1, -y + 2, z - 1/2$. [e] Atom generated with symmetry operation $-y + 2, -x + 1, -z + 1/2$.

The crystallographic data and selected bond distances and bond angles are listed in Tables 1 and 2, respectively.

Results and Discussion

The crystal structure of **1** consists of two different arrays of nets. The nodes of the nets are defined by two crystallographically independent iron sites denoted Fe1 and Fe2 located on a 2-fold symmetry axis. Figure 1 displays the molecular structure of Fe1. Iron atoms present similar coordination surroundings. They lie in a compressed octahedron with two *trans*-isothiocyanate ligands occupying the axial positions and four pyridine nitrogen atoms building the basal plane [Fe(1)−N(1)CS = 2.047(4), Fe(1)−N(2)(pyridine) = 2.271(3), and Fe(1)−N(3)(pyridine) = 2.250(4) Å; Fe(2)−N(21)CS = 2.052(7), Fe(2)−N(24)CS = 2.294(10), Fe(2)−N(22)(pyridine) = 2.270(5), and Fe(2)−N(23)(pyridine) = 2.284(6) Å]. The occurrence of disorder in the NCS^- groups is the main cause of the significant and uncommon difference between the Fe(2)−N(21) and Fe(2)−N(24) bond distances and induces departure from linearity for the NCS^- groups (average NCS^- angle of ca. 150°). Despite this fact, the structural data reported here are in good agreement with those available for other pyridine- and polypyridine-related spin crossover compounds.[6−8,14] The four pyridine units associated with each metal atom are arranged in propeller fashion (dihedral angles of 69.8 and 64.9° for the Fe1 and Fe2 centers, respectively). Each bpb ligand connects two iron atoms defining large [Fe_4] squares (Figure 2a). The edge-shared squares define the net structures with all the iron atoms, either coplanar (**A** set, Fe1) or slightly corrugated (**B** set, Fe2) (Figure 2b). The iron-to-iron separation through the bpb ligand is 16.628 and 16.393 Å for the **A** and **B** nets, respectively.

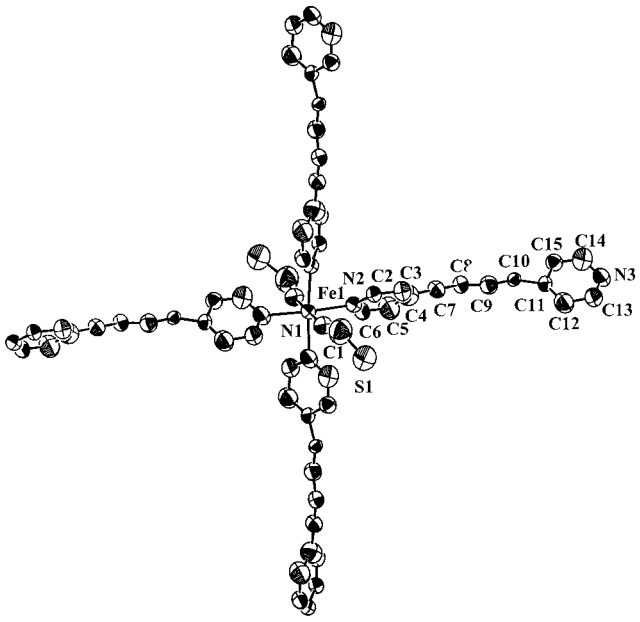

Figure 1. ORTEP diagram of **1** (30% ellipsoids).

A is made up by an array of parallel sheets stacked along the [001] direction. The sheets are slipped so that they form sequences of four nonsuperimposable sheets per unit cell (Figure 2b). **B** consists of two perpendicular stackings, organized along the [110] and [−110] directions, of interlocked square-grid sheets (denoted $\mathbf{B}_1$ and $\mathbf{B}_2$ subsets); the iron atoms lie in the holes of the grids of **A**, somewhat shifted from the centers of the holes. The iron atoms of $\mathbf{B}_1$ and $\mathbf{B}_2$ alternatively fill the holes of successive sheets of **A**. Two iron atoms of a [Fe_4] **B** square fill two holes of two equivalent **A** sheets ($\mathbf{A}_1$ and $\mathbf{A}'_1$) separated by $c = 22.7800(10)$ Å. The other two iron atoms lie in holes of the same **A** sheet halfway between $\mathbf{A}_1$ and $\mathbf{A}'_1$ (Figure 2b).

Each [Fe_4] square of a sheet, that is, $\mathbf{B}_1$ stack, has two rods of two consecutive parallel $\mathbf{B}_2$ stacks passing through it (Figure 2c). The **A** set penetrates the **B** set in such a way that each **B**-[Fe_4] hole is also meshed by three consecutive **A**-[Fe_4] squares. In addition, each **A** hole is also meshed by two [Fe_4] squares belonging to $\mathbf{B}_1$ and $\mathbf{B}_2$ subsets. This intricate situation is illustrated in Figure 2d. The solvent molecules, located close to the Fe1 coordination site, display significant short intermolecular contacts (2.7−4 Å) with the pyridyl rings.

The high-spin (HS) ↔ low-spin (LS) crossover behavior was monitored by measuring the temperature dependence of the

(14) (a) Roux, C.; Zarembowitch, J.; Gallois, B.; Granier, T.; Claude, R. *Inorg. Chem.* **1994**, *33*, 2273. (b) Claude, R.; Real, J. A.; Zarembowitch, J.; Kahn, O.; Ouahab, L.; Grandjean, D.; Boukheddaden, K.; Varret, F.; Dworkin, A. *Inorg. Chem.* **1990**, *29*, 4442. (c) Gallois, B.; Real, J. A.; Hauw, C.; Zarembowitch, J. *Inorg. Chem.* **1990**, *20*, 1152. (d) Konno, M.; Mikami-Kido, M. *Bull. Chem. Soc. Jpn.* **1991**, *64*, 339. (e) Real, J. A.; Gallois, B.; Granier, T.; Suez-Panamá, F.; Zarembowitch, J. *Inorg. Chem.* **1992**, *31*, 4972. (f) Real, J. A.; Muñoz, M. C.; Andrés, E.; Granier, T.; Gallois, B. *Inorg. Chem.* **1994**, *33*, 3587. (g) Ozarowski, A.; McGarvey, B. R.; Sarkar, A. B.; Drake, J. E. *Inorg. Chem.* **1988**, *27*, 628. (h) Moliner, N.; Muñoz, M. C.; Létard, S.; Létard, J. F.; Solans, X.; Burriel, R.; Castro, M.; Kahn, O.; Real, J. A. *Inorg. Chim. Acta* **1999**, *291*, 279.

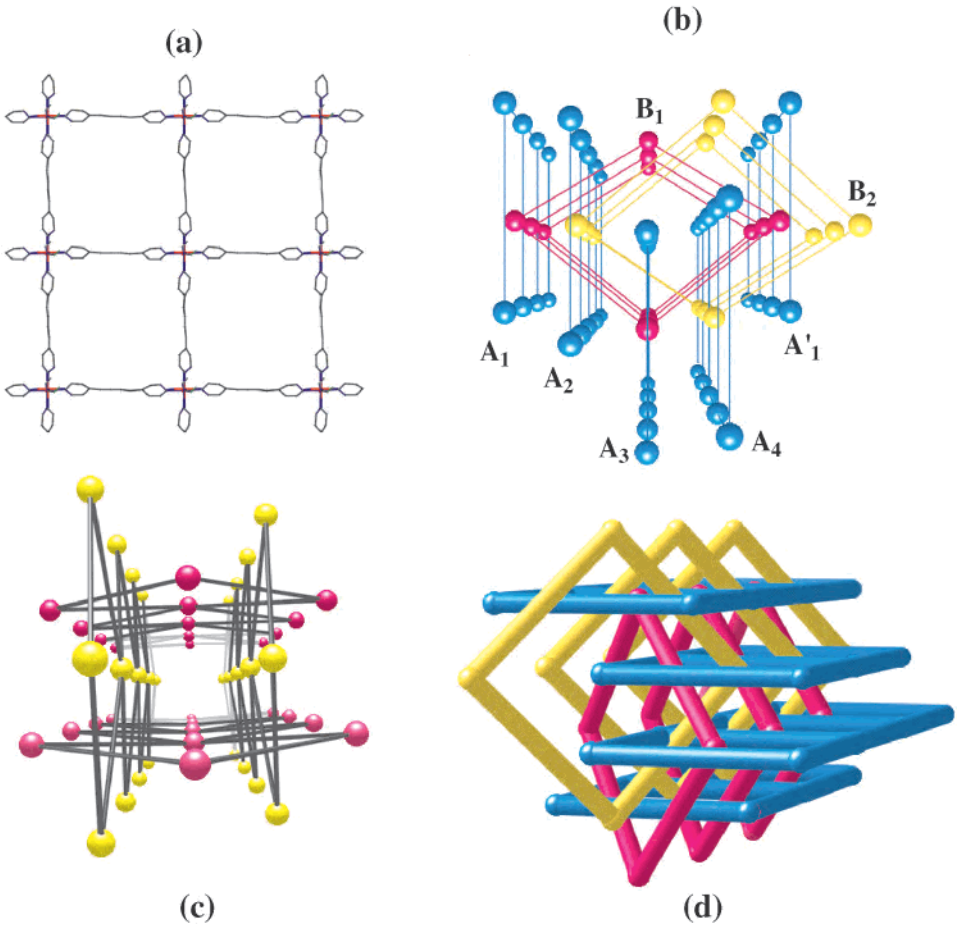

Figure 2. (a) Perspective view of a square-grid fragment. (b) Section of the crystal structure of **1** seen along the [100] direction, emphasizing the different sets of stacks: set **A** (blue) and set **B** (yellow and pink). (c) The interpenetration in the **B** system. (d) The interpenetration of the **A** and **B** arrays.

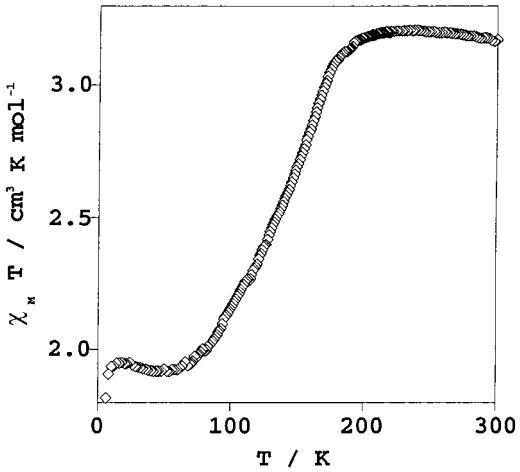

Figure 3. Thermal variation of $\chi_M T$ obtained from magnetic susceptibility measurements of **1**.

molar magnetic susceptibility, χ_M, and the Mössbauer spectra. The product $\chi_M T = 3.2$ cm^3 mol^{-1} K (T is the temperature) remains practically constant from room temperature to ca. 200 K, indicating that the sample is in the HS ground state. $\chi_M T$ decreases gradually upon cooling because of the HS → LS conversion and reaches a plateau around $\chi_M T = 1.9$ cm^3 mol^{-1} K at 60 K (Figure 3). The further decrease observed below 20 K, when cooling, indicates that zero-field splitting occurs in the $S = 2$ ground state of the remaining HS molecules at low temperatures. No thermal hysteresis is observed. The temperature evolution of the Mössbauer spectra shown in Figure 4 agrees with the magnetic data. The dominant doublet observed at room temperature, characterized by the quadrupole splitting $\Delta E_Q = 2.453$ mm s^{-1} and the isomer shift $\delta = 1.006$ mm s^{-1}, corresponds to the HS ground state of iron(II). The small doublet characterized by $\Delta E_Q = 0.716$ mm s^{-1} and $\delta = 0.334$ mm s^{-1}

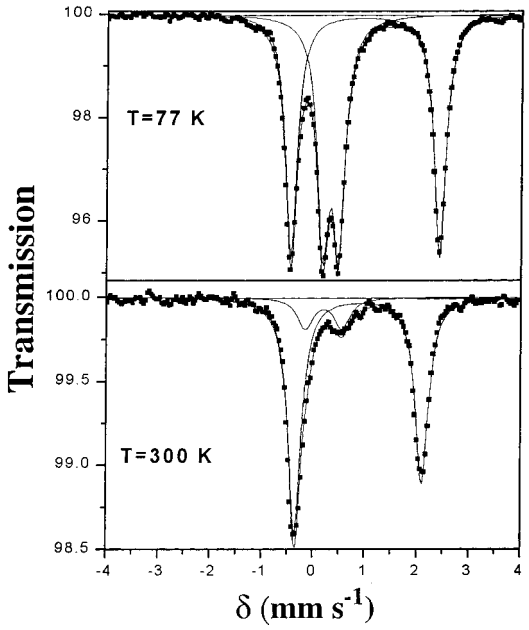

Figure 4. Mössbauer spectra of **1**.

corresponds to 14.78% of LS molecules remaining at room temperature. As the temperature is lowered, the intensity of the LS doublet increases at the expense of that of the HS doublet. The fitted parameters at 77 K are $\Delta E_Q = 1.12$ mm s^{-1} and $\delta = 2.87$ mm s^{-1} for the HS species and $\Delta E_Q = 0.462$ mm s^{-1} and $\delta = 0.308$ mm s^{-1} for the LS species, occurring in almost equal amounts.

There are some well-documented iron(II) spin crossover compounds for which incomplete spin conversion at low temperatures has been observed. For instance, $[Fe(mtz)_6]X_2$ (mtz = 1-methyltetrazole and X = ClO_4^- and BF_4^-) present two distinct iron(II) sites distributed in equal amounts in the crystal.[15] One site undergoes LS ↔ HS spin conversion, whereas the other remains HS throughout the temperature range.[16,17] A similar behavior has been observed for $[Fe(etz)_6](BF_4)_2$ (etz = 1-ethyltetrazole) in which the site population Fe1:Fe2 is 2:1. Complexes on the Fe1 site show thermal spin conversion in contrast to those on the Fe2 site, which remain high spin.[18]A 50% spin conversion was also observed in the binuclear {[Fe(bpym)$(NCSe)_2]_2$bpym}. The occurrence of half-spin transition in this compound was attributed to the interplay between intramolecular interactions favoring the mixed-spin {HS−LS} molecular state and intermolecular interactions favoring like-spin ({LS−LS} or {HS−HS}) species domains.[19]

The occurrence of 50% spin conversion in **1** can be related to the presence of two iron(II) sites in the crystal, as for the above-mentioned Fe^{II}-Rtz derivatives. The Fe1 site is prone to undergo spin conversion as it exhibits metal-to-ligand bond distances slightly shorter than those of Fe2. Solvent molecules may influence the ligand field experienced by the iron atoms. In fact, the Fe1 site presents intermolecular contacts with the methanol molecule that are more numerous and intense than those of the Fe2 site.

The main two points of this work are the unprecedented supramolecular architecture and the occurrence of half-spin transition. Half-spin transitions are fascinating because they can be viewed as two-step spin transitions, the low-temperature step of which is missing, for various (static or dynamic) reasons. For instance, the missing HS ↔ LS conversion in $[Fe(etz)_6](BF_4)_2$ has been photoinduced[18] by use of the reverse LIESST (light-induced excited spin state trapping) technique, and the application of pressure revealed the occurrence of a two-step spin transition in {[Fe(bpym)$(NCSe)_2]_2$bpym}.[20] In a similar way, we intend to further investigate the control of the spin crossover regime of **1** through light irradiation and pressure experiments.

Acknowledgment. This research was supported by the Spanish Dirección General de Investigación Científica y Técnica (DGICYT) (Project PB97-1397) and the European Commission (TMR-Network "Thermal and Optical Switching of Molecular Spin States (TOSS)", Contract No. ERB-FMRX-CT98-0199EEC/TMR).

Supporting Information Available: Tables of X-ray crystallographic data in CIF format for **1**. This material is available free of charge via the Internet at http://pubs.acs.org.

IC0005588

(15) Wiehl, L. *Acta Crystallogr*. **1993**, *B49*, 289.
(16) Poganiuch, P.; Decurtins, S.; Gütlich, P. *J. Am. Chem. Soc*. **1990**, *112*, 3270.
(17) Buchen, T.; Poganiuch, P.; Gütlich, P. *J. Chem. Soc., Dalton Trans*. **1994**, 2285.
(18) Hinek, R.; Spiering, H.; Schollmeyer, D.; Gütlich, P.; Hauser, A. *Chem.—Eur. J*. **1996**, *2*, 1127.
(19) Real, J. A.; Castro, I.; Bousseksou, A.; Verdaguer, M.; Burriel, R.; Castro, M.; Linares, J.; Varret, F. *Inorg. Chem*. **1997**, *36*, 455.
(20) Gaspar, A. B.; Real, J. A.; Ksenofontov, V.; Levchenco, G.; Spiering, H.; Gütlich, P. Unpublished results.